

## “Bragg Peak Sensing”, a New Method for Catalysis Research?

Walter Vogel\*

National Central University, No. 300 Jung-Da Rd., Chung-Li, Taoyuan, Taiwan 32001

**Corresponding Author:** Walter Vogel, National Central University, No. 300 Jung-Da Rd., Chung-Li, Taoyuan, Taiwan 32001. Tel.: +886 972505210, E-mail: vogelw@ncu.edu.tw

**Citation:** Walter Vogel (2023) “Bragg Peak Sensing”, a New Method for Catalysis Research?. Int J Cat 2: 1- 17

**Copyright:** © 2023 Walter Vogel. This is an open-access article distributed under the terms of Creative Commons Attribution License, which permits unrestricted use, distribution, and reproduction in any medium, provided the original author and source are credited.

### Abstract

The demand for surface sensitive techniques in catalysis and nano-science is high. In this paper the possibility of monitoring X-ray Bragg reflection intensity of a metal catalyst as a probe of high surface sensitivity is shown. This is related to the high fraction of atoms exposed, e.g. 50 % for a 2 - 3 nm platinum particle. Nano-divided metal particles exposed to air will usually develop an amorphous oxide layer. Atoms not in registry with the core of the nanoparticle do not contribute to the coherently scattered intensity. The signal measured at the center of the Bragg peak drops. For the first time a method applicable in normal lab- scale experiments is here presented, allowing to measure dynamic surface restructuring of nanoparticles at atmospheric pressure under reaction conditions (*in-operando*). Gas phase CO oxidation over a commercial platinum catalyst was studied as a suitable test reaction. The experiment's method grants a direct view of the surface dynamics during the temperature and pressure dependent reaction and ignition processes. It also allows a detailed insight into the scenario at the bi-stability region, switching between high activity (high oxide coverage), and low activity (low oxide coverage). The data give evidence of the partial oxidized platinum surface being the most active phase. It becomes apparent that the Pt particles behave in a collective way, possibly related to the fractal topography of the porous carbon support.

**Keywords:** in-operando PXRD, CO oxidation, E-TEK Pt/Vulcan XC-72

## Introduction

It has been accepted and confirmed by a series of papers, that surface oxide formation is crucial for a high activity at realistic high-pressure conditions of CO oxidation over supported platinum and ruthenium catalysts [1-5]. A variety of techniques applicable under in situ conditions were used: X-ray absorption spectroscopy [1,6], infrared spectroscopy [6-11], X-ray diffraction [12]. Synchrotron-based experiments have been conducted, which combine several techniques in one in situ set-up to study chemical processes in action [1, 13].

Here we demonstrate a new approach of potential value in surface science of nano-systems. Coherent X-ray diffraction, which is volume sensitive by nature, becomes surface sensitive for highly dispersed particles. The coherently diffracted X-ray total intensity into a Bragg reflection is proportional to the volume of the scattering crystallite, as long as its size is small enough to neglect absorption<sup>1</sup>. For an assembly of nano-crystals within an irradiated volume with different sizes each particle  $v$  with mass  $m_v$  scatters independently, each contributing a fraction  $i_v = k m_v$  to the Bragg peak. The total integral intensity of a Bragg peak<sup>2</sup> is therefore

$$I = \sum i_v = k \sum m_v = kM$$

The total mass  $M$  would not change if, for instance, the average size increases by coalescence of the primary particles. M. v. Laue [14], and later Wilson [15] have shown, that the volume averaged crystallite size is given by  $\bar{V} = I_0 / I$ , where  $I_0$  is the intensity at the peak of the Bragg profile. Measuring the change in the peak intensity scattered from a constant volume of a catalyst therefore relates to change in the mean particle size within this volume. This kind of change is irreversible. However, other processes can produce reversible intensity changes, for example surface oxidation and surface oxide reduction. If surface oxide has been formed, it scatters incoherent with the metallic core. In this case, the total mass of atoms in registry with the core crystallites is in fact less, and the Bragg intensity must be lowered. The surface oxide, which is usually amorphous [16,17], only contributes diffuse intensity to the background. The fraction of atoms converted to surface oxide species can be quantified, if proper care is taken to correct for all background contributions [20]. The conditions of the experiment and the history of the sample under investigation in general determine unambiguously, whether an increasing Bragg peak intensity is related to particle growth or reduction of surface oxide. The actual and unique strength of method is in fact the ability to distinguish both, surface changes as well as particle growth in a single experiment. The term "Bragg Peak Sensing" introduced here defines experiments described above, though have in the past not been conducted under a common header [12, 17-20]. Here we apply this technique to monitor the CO oxidation over a commercial carbon-supported platinum catalyst.

An immense work has been devoted to study this apparently simple catalytic reaction. Langmuir [21] in 1922 posted a paper, saying, "Variations of the topography of the surface during reaction are observed". It was soon accepted that CO oxidation over Pt is performing *via* the Langmuir-Hinshelwood (LH) mechanism [22]. In the past the majority of studies have been focused on single crystals under UHV conditions [2, 23-27]. Ertl has pointed to the importance of a subsurface oxygen phase for CO oxidation on single crystals of Pd, but has not been observed on Pt [26]. Ackermann et al. [5] studied CO oxidation on Pt (110) at pressures up to 0.5 bar using surface X-ray diffraction, and report two different thin surface oxides, commensurate and incommensurate. Both oxides have a substantially higher catalytic activity than the bulk-terminated Pt surface. In Reactor-STM experiments at high O<sub>2</sub> pressure (1-5 bar) oxide formation on Pt (111) revealed ordered surface oxide deposits at higher pressure and temperature, but disordered worm-shaped islands at 1 bar O<sub>2</sub>, 18 – 65 °C [28]. In another study on curved Pt (111) single crystal surfaces minor amounts of oxygen were observed present in a CO-poisoned layer, and a build-up of subsurface oxygen within Pt (111) terraces [29].

CO oxidation experiments on 2 nm Pt nanoparticles supported on spherical silica by *in situ* DRIFT experiments gave evidence for a surface oxide formation [30]. Very recent CO oxidation experiments were performed by Lashina et al. [31] on 2.5 nm Pt nanoparticles supported on carbon nanotubes (MWCNTs).

Beside the metallic Pt4f doublet, the XPS spectrum of the used catalyst shows two extra doublets related to the oxidized species  $Pt^{2+}$ ,  $Pt^{4+}$ . Their fraction relates to 30% of the overall Pt4f spectrum.

Turner, Sales and Maple [32] were the first to postulate subsurface oxide formation as the driving force for the oscillating behavior at high pressures of the reaction rate over Pt wires. They derived a simple kinetic model based on this hypothesis [32, 33], which is in qualitative agreement with the experiments. This oxide model for rate oscillations of CO oxidation has been then confirmed by many groups [7, 8, 12]. The question of the active sites is still controversial, and some authors believe the active surface is metallic Pt [6,12]. It has been shown in 1994 that non-isothermal rate oscillations of CO oxidation over a supported Pt catalyst are accompanied by a periodic intensity variation of the Bragg peaks [12]. Further, it has been proved, that these changes are related to a periodic oxidation and reduction of the catalyst surface. Such rate oscillations were observed even under totally isothermal conditions, and in the absence of mass transport limitations [7, 8]. For supported catalysts, heat and mass transport limitations usually render a quantitative description of oscillation more difficult.

## Experimental

The X-ray experiments are based on a commercial Guinier diffractometer (Huber), set to 45° transmission mode, with a focused primary beam of Cu-K $\alpha_1$  radiation ( $\lambda = 1.5406 \text{ \AA}$ )

The standard sample holder was replaced with a homemade in situ reaction cell [12, 34] (Figure. S2, S3, supporting information). A special designed software is used for the remote control the system, which allows the operation in specific modes, making it a versatile tool for catalysis studies. Catalytic *in operando* studies presented in this work were performed in the "open slit" (OS) mode: the detector is placed stationary at a specific Bragg peak, with a wide receiving slit (typically  $\pm 0.5^\circ$  theta). Changes in the Bragg peak intensity are monitored versus treatment conditions [12, 19, 20, 35]. The diffracted intensity at the Pt-111 peak (typically  $\sim 10^4$  c/s) is sufficiently high to achieve information on a time scale of 5 - 10s. A quadrupole mass spectrometer (QMS, VG) is attached through a differentially pumped transfer line. Two mantle thermocouples (TC's, o.d. 0.5 mm) are connected to the sample holder and the catalyst pellet surface, respectively. The operating system collects the different synchronized signals within a pre-selected time interval. The catalyst in a powder form is slightly pressed into a thin pellet and sandwiched between two 0.1 mm Be platelets. The gases used for the experiments are of purity 5 and were used without further purification. Before the catalytic measurements the cell was evacuated for about one hour to a base pressure of  $10^{-3}$  mb.

The catalyst used for the present study is a commercial product, a 20 wt.% Pt/C (E-TEK). It is frequently used as a reference catalyst in fuel cell application, and has been well characterized [20, 36-39]. The 2-3 nm Pt particles expose a surface area of  $110 \text{ m}^2/\text{g}$  [36, 38], and are well dispersed on highly porous amorphous carbon (Vulcan XC-72R). The carbon BET surface area is  $235 \text{ m}^2/\text{g}$ , and the volume of meso-macropores is  $0.52 \text{ cm}^3/\text{g}$ , with a maximum of the pore size around 30 nm [36].

## Results

### Pretreatments, Figure 1,2,3

Bragg diffraction is a perfect probe of surface oxide, as demonstrated in Figure 1. Reduction of oxides on a platinum surface proceeds fast and at room temperature, by injecting a pulse of  $H_2$  into the evacuated cell. A small up-step of the Pt-111 peak intensity ( $I\text{-signal}^3$ ) is induced as seen in Figure 1<sup>4</sup>. Exposure with 100 mb of  $H_2$  induces full reduction and a remarkable increase of the I-signal of 24%, in good agreement with XPS results [38].

X-ray scans performed before, -and after  $H_2$ -exposure give further evidence for the successful reduction (Figure 2): Diffuse scattering produced by amorphous oxide species is removed, and the coherent scattering of the Pt particles increases. Annealing in vacuum can be used to decompose the surface oxide species, as well [unpublished data].

The Pt-111 intensity increases by the same magnitude (22%). The temporal gradient of the I-signal correlates to the rate of surface oxide dissociation and goes through a maximum at around 140 °C. A consecutive H<sub>2</sub>-exposure has no effect on the I-signal, thus providing evidence for complete removal of surface oxide. Surface oxides formed on bulk platinum is known to dissociate at considerably higher temperature (400-600 °C) [40, 41]. The quadrupole mass spec. attached to the in-situ cell provides the option to measure the temperature induced desorption of pre-adsorbed surface species. Figure 3 shows the removal of surface-bonded hydrogen to provide a clean platinum surface for the consecutive CO oxidation experiments. Hydrogen is known to be weakly bound to the platinum surface. Here the maximum of hydrogen desorption was observed at around 60 °C<sup>5</sup>.

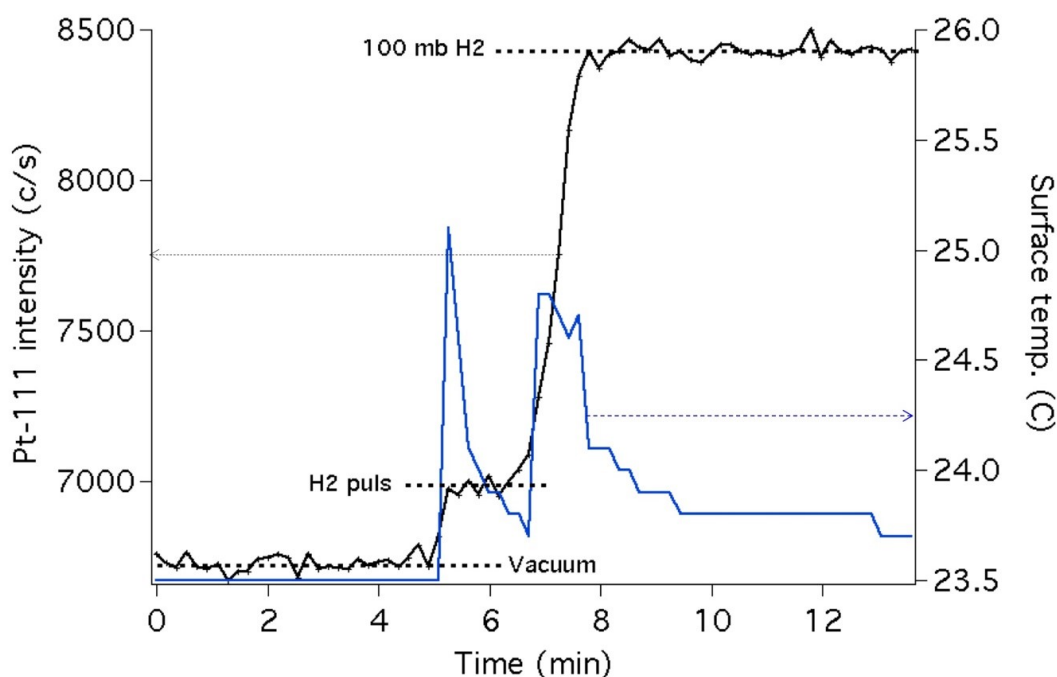


**Figure 1:** Pretreatment of the as-received Pt/C catalyst in hydrogen versus the platinum-111 peak intensity (I-signal). First step: injection of a pulse of H<sub>2</sub> under dynamic vacuum. Second step: exposure to 100 mb of H<sub>2</sub>. The detector set stationary  $\Theta = 19.85 \pm 0.5^\circ$  (see Figure 2). Small exothermic variations of the catalyst surface temperature are also observed.

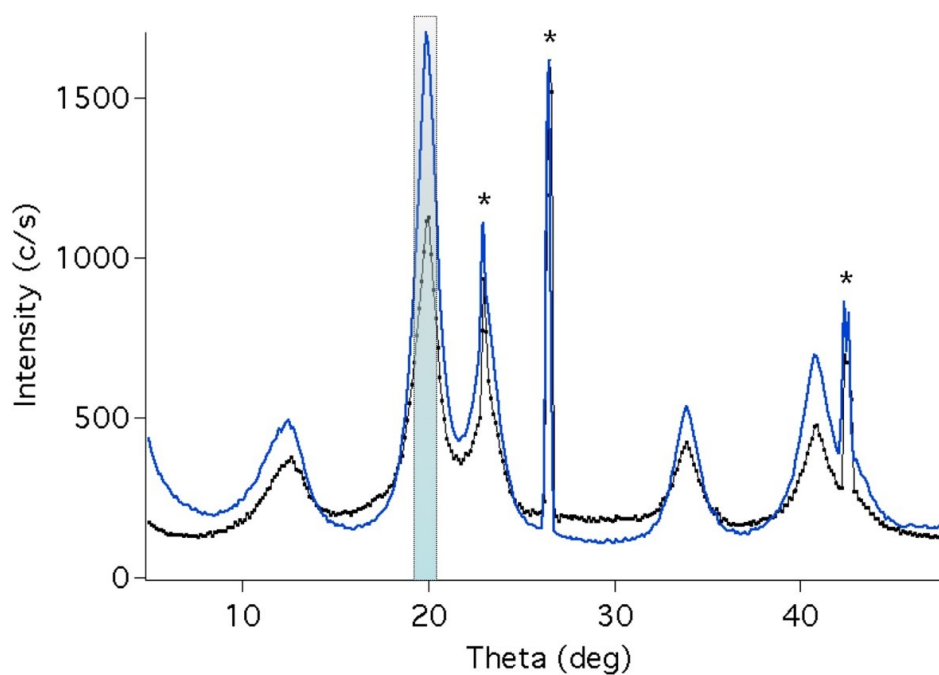


**Figure 2:** X-ray scans before (black line) and after reduction in H<sub>2</sub> (blue line). Intensities are comparable on an absolute scale. The colored bar marks the “Bragg Window” for the OS measurement shown in Figure 1. Peaks marked by an asterisk are beryllium reflections. The diffuse peak at  $\Theta \approx 12^\circ$  is produced by the carbon support.

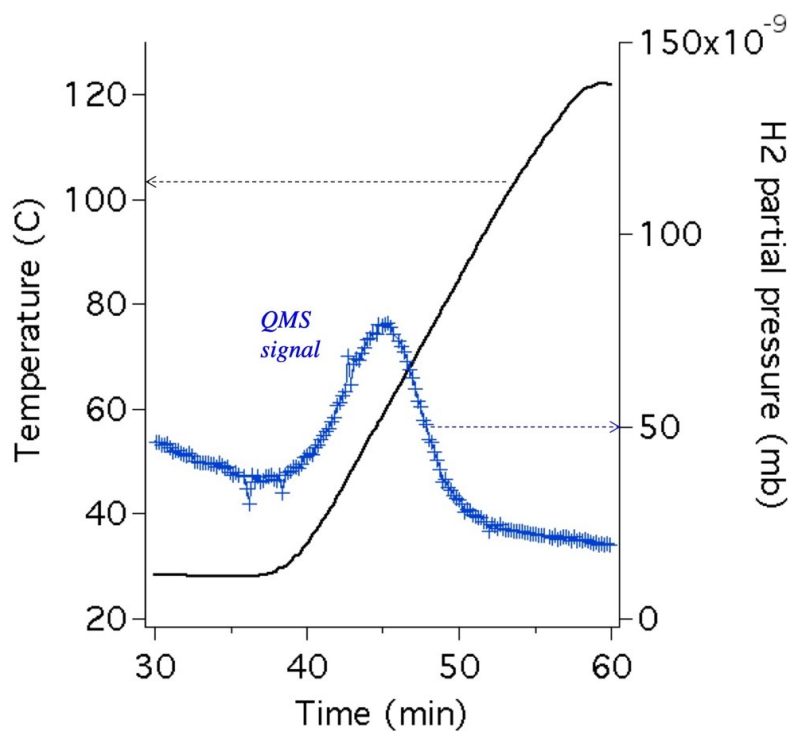


**Figure 3:** The reaction cell is used for a temperature programmed desorption (TPD) experiment, by heating under vacuum to remove hydrogen from the platinum surface. H<sub>2</sub> desorption appears around 60 °C.

## Oxidation of Pre-Adsorbed CO, Figure 4

The reduced catalyst was exposed to 18 mb of CO at a base temperature<sup>6</sup> of 80-100 °C to produce a saturation coverage of CO on the Pt surface, followed by evacuation and introduction of a flow of oxygen (11 ml/min). The temperature was ramped to a maximum 270 °C, sufficiently high to promote thermal desorption of CO from the Pt surface (red line). The I-signal begins to drop above  $T = 150\text{ °C}$ <sup>7</sup> (Point 1 in the Figure). According to the statements made in the introductory part we conclude, that an oxide phase begins to form at the catalyst surface. Importantly, here we have to consider two competing processes: particle growth on annealing raises the I-signal, while oxide formation lowers the I-signal. This compromises to quantify the amount of oxide being formed: The total drop of the I-signal measured from Figure 4 is ~ 8%, but might be higher to an unknown amount.

It appears that oxygen can react with the Pt surface, even though surface-bond CO molecules cover the particles. CO desorption would be seen as an increasing  $p(\text{CO}_2)$ -signal (green line) at this point<sup>8</sup>. In this context it is of interest that no signs of a catalytic ignition occurs with CO pre-adsorbed, instead of being supplied by the gas phase. Typically, ignition would be observed between 150- 260 °C for CO oxidation over platinum [27].

Formation of  $\text{CO}_2$  in the gas phase occurs above  $T > 150\text{ °C}$ , as the  $\text{CO}_2$  partial pressure begins to increase (green line). Certainly, there is diffusion-induced delay of the  $\text{CO}_2$  signal, caused by the supporting carbon. At the actual experimental conditions progressive surface oxidation by oxygen is apparently associated with a gradual increase of CO oxidation via Langmuir-Hinshelwood (LH) mechanism. The  $\text{CO}_2$  pressure goes through a maximum (Point 3) with a delay of  $\approx 6$  min, after lowering (Point 2) the temperature from 280 to 200 °C. This 6 min delay may be representative for the mean diffusion time of  $\text{CO}_2$  molecules to exit through the pellet's surfaces.

An abnormal and unexpected discontinuity of the  $\text{CO}_2$  signal is observed at point 4 in Figure. 4. The  $\text{CO}_2$  partial pressure drops to the base pressure of the QMS within  $\approx 40$  s (see Figure S6, supporting information). The phenomenon can be best understood by a collective coupling among individual platinum particles, as described by Tinsley et al. [42] for Langmuir-Hinshelwood reactions. If the particles deplete their CO reservoir synchronously, the last  $\text{CO}_2$  molecules released from the catalyst particles diffuse through the carbon support to the surface of the catalyst pellet, and the QMS signal should in fact fall off quickly.

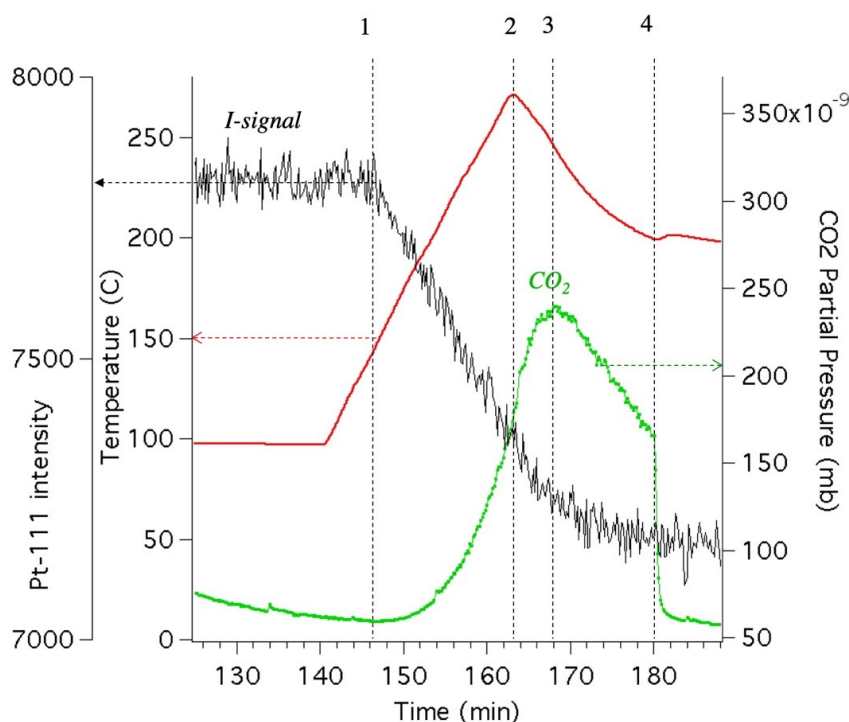


**Figure 4:** OS-experiment of the reduced catalyst, after pre-coverage with CO (18 mb) at 100 °C, followed by evacuation and exposure to a flow of oxygen. Annealing is ramped to max. 270 °C. Note the decrease of the I-signal, beginning at 150 °C ( $t_i$ ). An unexpected fast drop of the  $\text{CO}_2$  signal occurs at ( $t_d$ ).

Kopelman [43] has discussed “fractal reaction kinetics” in systems with fractal topography, which may apply to the catalyst under investigation. In fact, the fractal surface dimensionality  $D_s$  of the carbon support material was shown to be very high,  $D_s = 3.6$  (unpublished data).

In terms of surface science, the following interpretation can be proposed: Above 150 °C some CO molecules begin to desorb leaving free Pt surface sites.  $\text{O}_2$  can chemisorb at this site by dissociation into two oxygens.

One oxygen atom reacts with a neighboring CO to desorb as free  $\text{CO}_2$  molecule via the LH-mechanism, while the second oxygen may react to form some  $\text{PtO}_x$  species. If this process goes on, a new platinum oxide phase can form locally and at the same time a  $\text{CO}_2$  gas phase builds up. It is assumed that the CO coverage of the Pt surface is progressively reduced at a rate dependent on the temperature. The rate of CO oxidation accelerates with the increasing temperature. Previous to point 4 of Fig. 4 the total available platinum surface was depleted from CO by the LH-reaction. Apparently, this requires some synchronization among individual Pt nanoparticles over a scale of centimeter. If this occurs a final “cloud” of  $\text{CO}_2$  travels through the carbon support to the pellet surface.

### CO Oxidation Activity Versus Gas Composition, Figure 5

The now partially oxidized catalyst (~ 8%, as determined from the change of the Pt-111 peak intensity in Figure 5) was exposed to a flow of the reactants with decreasing ratios of oxygen to carbon monoxide (ratios shown at the bottom of the Figure). Again, the Pt-111 peak intensity (black noisy line) is used to monitor the platinum surface oxide. The total flow rate (220 ml/min) and the base temperature of 205-215 °C were kept constant in this experiment.

Both, the surface excess temperature and the CO<sub>2</sub> partial pressure were used as tracers for the catalytic activity. Figure 5 shows the two signals (black and green line, respectively) versus reaction time. It is evident, that the response time of the surface temperature, induced by switching partial pressure of the reactants, is much faster than that of the diffusion limited CO<sub>2</sub> signal. The partial pressures of O<sub>2</sub> and CO are included as blue and red lines, respectively<sup>9</sup>. Starting with an excess of oxygen (O<sub>2</sub>:CO = 9:1), the activity increases with increasing CO to a maximum at the stoichiometric ratio of 1:2. However, at this point, after an induction period of 330 sec the activity drops spontaneously to a lower level. The reason is evident from the change in the observed Pt-111 peak intensity: at the actual conditions of temperature and partial pressures the highly oxidized surface becomes unstable, and is rapidly reduced. The I-signals up-step is ~33% at this point, which relates to the true fraction oxide formed in due process. Such high oxide fractions of 30% were also deduced from XPS spectra of a Pt/C catalyst [31]. The catalyst was held at temperatures above 210 °C for a period of 2 hours, certainly inducing a steady particle growth during that period.

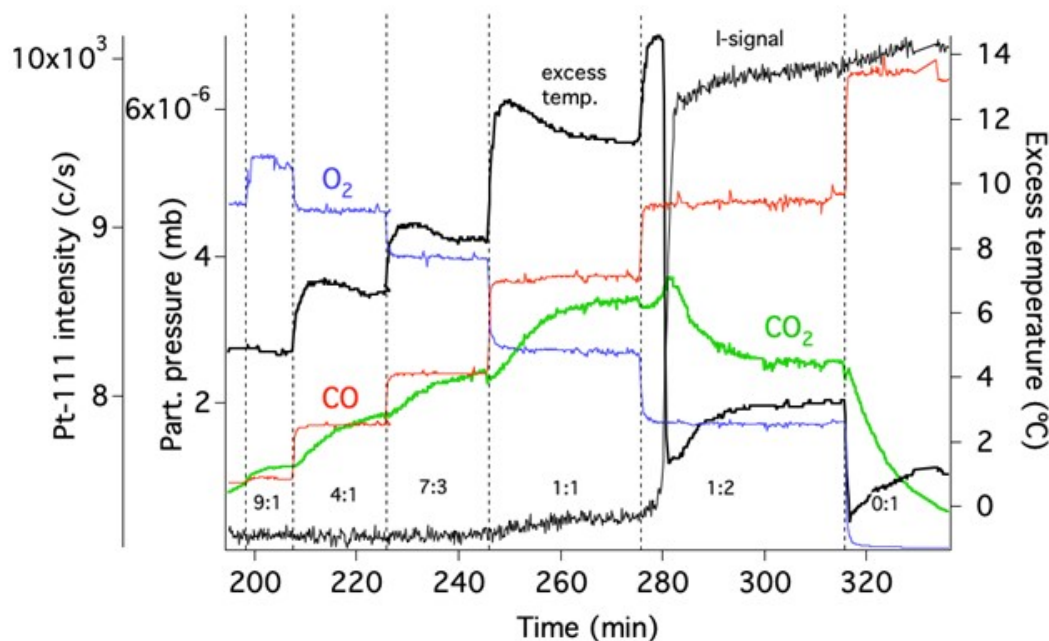


**Figure 5:** This is a follow-up of the previous OS experiment, with the catalyst kept in a state of partial surface oxidation and at a constant base temperature around 210 °C. The catalyst is exposed with a flow of reactants at varying ratios of O<sub>2</sub>:CO as indicated in the figure (total flow rate kept constant). The CO<sub>2</sub>-signal has been amplified by a factor of 10.

Therefore, the overall increase of the I-signal from starts in Figure 4 to the end in Figure 5 (both are in the reduced state) amounts to ~28%, a number solely related to particle growth. It remains an open question if the observed fast reduction proceeds as a synchronous collective event, or perhaps propagates as wave-like spatiotemporal reaction front [44]. In a final step the oxygen flow was shut off, and the reaction is aborted. The slow drop of p(CO<sub>2</sub>) to the base pressure is again affected by diffusion limitation and residual oxygen present inside the catalyst pellet after O<sub>2</sub> shut off, which still provides fuel for CO oxidation.

### Bi-stability and Collective Processes, Figure 6

At a fixed temperature the catalyst can be switched between two states: an oxidic surface state, and a reduced surface state. The change can be controlled by switching the gas composition CO:O<sub>2</sub> from 1:1 to 2:1, as shown in the figure. The base temperature was held at ~250 °C in this experiment (dotted green line). The catalyst surface temperature (red line) is synonymous for the catalyst's activity. Whenever the gas composition is changed, the catalysts activity increases up to a critical temperature. Once this point is reached<sup>10</sup>, a spontaneous and fast reversal of activity is induced by either surface oxidation (low CO pressure), or surface reduction (high CO pressure). In either case the activity goes down to approach to a steady state. Evidently the activity in the steady state is higher for the oxidized surface as compared for the reduced surface.

We believe that in the reduced state the CO coverage must reach a limit, low enough for oxygen to chemisorb on free platinum sites, and to immediately transform the surface into an oxide layer. The heat of reaction itself induces the reversal. Adversely, in a state of an oxidized surface and high CO pressure ( $\text{CO}:\text{O}_2 = 2:1$ ), a critical temperature is needed for CO to reduce the surface oxide. Note, that reduction proceeds fast until all oxide is reduced, as the intensity reaches a plateau. Conversely, the oxidation proceeds fast in a first step, but followed by a slower deep surface oxidation. There is a striking similarity of the I-signal (oxide coverage), and the T-signal (reaction rate) during oxide formation.

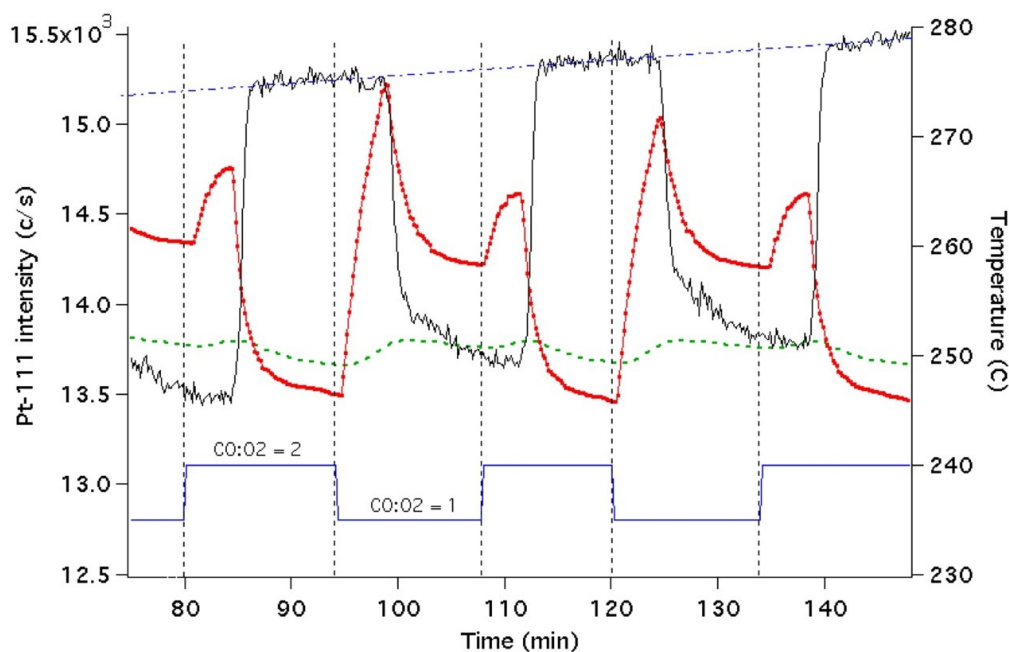


**Figure 6:** Base temperature held at constant 250 °C (green). Gas reactants switched periodically between excess CO ( $\text{CO}:\text{O}_2 = 2$ ), and equal molar ratio ( $\text{CO}:\text{O}_2 = 1$ ). Pt-111 intensity (black) and catalyst surface temperature (red).

We attribute the nearly spontaneous raise of the catalysts surface temperature after switching from high CO to low CO level to a non-equilibrium ignition-like processes: Oxygen reacts via LH mechanism with the CO, first on near-surface Pt particles, and the reaction front precedes to the interior of the sample. A similar but less pronounced non-equilibrium process happens when we switch from low to high CO ambient while the catalyst prevails in the surface-oxidized state, which induces an increase in reaction rate. The process lasts for the diffusion-limited period of  $\sim 4.5$  min, until CO coverage reaches a critical level. The sudden and fast increase of the I-signal (up to  $\sim 12.6\%$ ) resembles to a “switching” of the whole catalyst pellet into a state of oxide-free surface. The T-signal is inverted at this point, and approaches to a low-lying equilibrium value in this reduced state.

Some typical changes are related to the progressive growth of the particles in this experiment. Note, that the critical temperatures for surface oxide formation and reduction are decreasing with the number of cycles. Particle growth is also apparent from the linear increasing slope of the plateau-like intensity in the reduced state (dash-dotted line).

## Ignition Studies, Figure 7

A fresh catalyst was used to study the ignition process in detail. A flow of  $O_2:CO = 110:110$  ml/min was used in this experiment. The catalyst was first reduced, and consecutively exposed to CO at room temperature, followed by adding the oxygen flow. As the catalyst is pre-reduced, the initial increase of the I-signal cannot be caused by surface oxide reduction but by a temperature driven growth of the Pt particles. The base temperature (red line) was ramped to 250 °C. Ignition occurs at 210 °C, and induce two inter-correlated events: (i) a spike-like overheating: The surface temperature, - here shown as the excess temperature (blue line), i.e., the temperature above the base temperature, - rises to 170 °C within less than 10 sec<sup>11</sup>. It also drops back fast (~2 min), assisted by the high thermal conductivity of the carbon support; (ii) the flash-like temperature spike depletes the surface from CO, and lets oxygen to react with Pt surface atoms to form an amorphous surface oxide. This process of rapid (~60s) oxide formation is evident from the ~10% drop of the I-signal, in coincidence with the excess temperature. The  $CO_2$  partial pressure (not shown) raises from 1 to  $3.7 \times 10^{-7}$  mb at maximum ( $t = 155$  min).

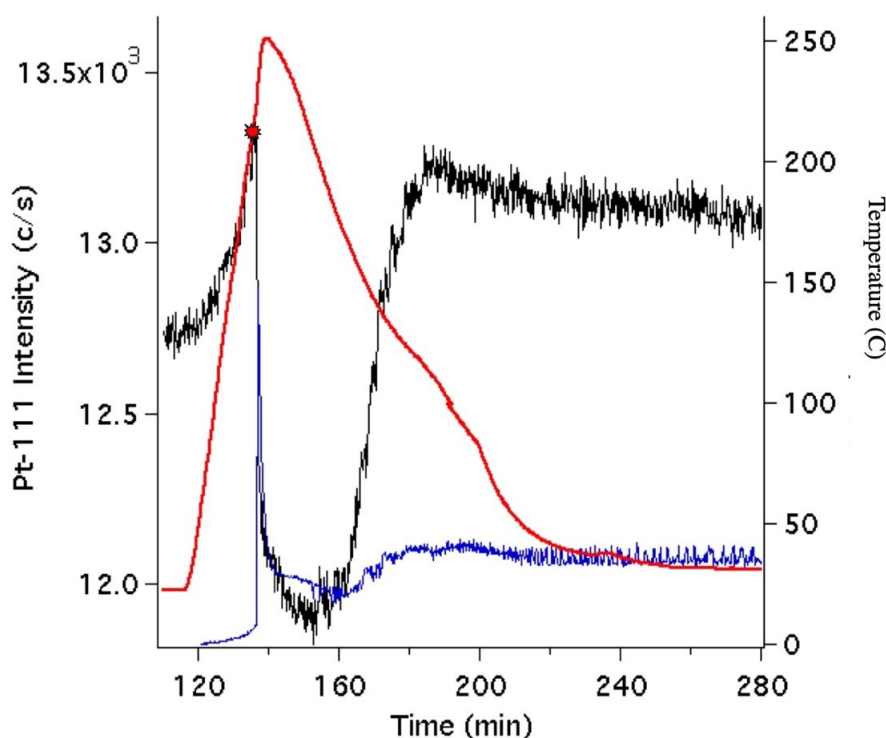


**Figure 7:** Ignition experiment in a flow of  $O_2:CO = 110:110$  ml/min. Base temperature (red), Excess temperature (blue), and Pt-111 peak intensity (black).

As the base temperature is slowly lowered, we observe a full reversal of the I-signal to the pre-ignition state. Such an increase of the Pt-111 peak intensity on down-cooling the catalyst can only be attributed to a progressive re-reduction of the ignition-induced surface oxide layer. The reversal is comparatively slow, and proceeds in an oscillatory behavior. Low frequency oscillations are also recognized in the surface temperature. Once the temperature reaches about 110 °C, a stationary reduction state was reached. Chaotic fluctuation of both surface temperature, and the intensity are prevailing. The latter signal is overlaid with a statistical noise, which partly covers chaotic fluctuations related to CO oxidation.

## Conclusion

The *in-operando* experiments presented here, (“Bragg-Peak Sensing”), open a new window for surface- sensitive studies on real catalytic systems under realistic high-pressure conditions (commonly noted as bridging the pressure, - and material gap). Its base is the observation of just one Bragg peak under varying conditions of treatment, as presented in the Figure 1, 4 to 7. E.g., Figure 5 shows the spontaneous flip from a high active, - oxide covered surface to a reduced surface state with low activity, triggered by a change in the reactant’s composition. This bi-stability behavior is also demonstrated in Figure 6: repeated switching from a high CO reactants mixture to a low CO composition. On every switch there is a diffusion-limited transition period with unexpected behavior. But in the steady state, CO oxidation activity is higher in the partial oxidized, than in the reduced state. Supply of the reactants in the gas phase (Figure 7) induce a massive ignition-caused overheating of the particles, and rapid surface oxidation. However, a catalyst pre-covered with CO under flowing oxygen (Figure 4) forms a slowly progressing oxidic surface at 150 °C with no signs of an ignition. The Pt particles seem to react in a collective mode via a macroscopic coupling, enforced by the fractal geometry of the supporting carbon material [45]. Without such a collective coupling, reduction of individual particles would slowly proceed along the gradient of the partial CO pressure inside the compressed pellet. Globally coupled dynamical systems are also widely used as prototypical models for addressing the collective behavior of systems with many degrees of freedom [43, 46-48]

## Supplementary Figures

### Some details about the modified *Guinier* system used for catalytic studies

#### Advantageous *Guinier* setup

The transmission setup of a *Guinier* diffractometer modified for in situ experiments is superior to the standard *Bragg-Brentano* system. The scattering volume (marked red) in the schematic Figure S1 is fixed and remains fixed through all sequential treatments performed on the catalyst material. Therefore, repeated angular scans are comparable on an absolute I-scale, before and after any selected treatments. This is evidently of great value. For the transmission case samples have to be thin, and both surfaces are exposed to gas ambient, in advantage to the *Bragg-Brentano* setup.

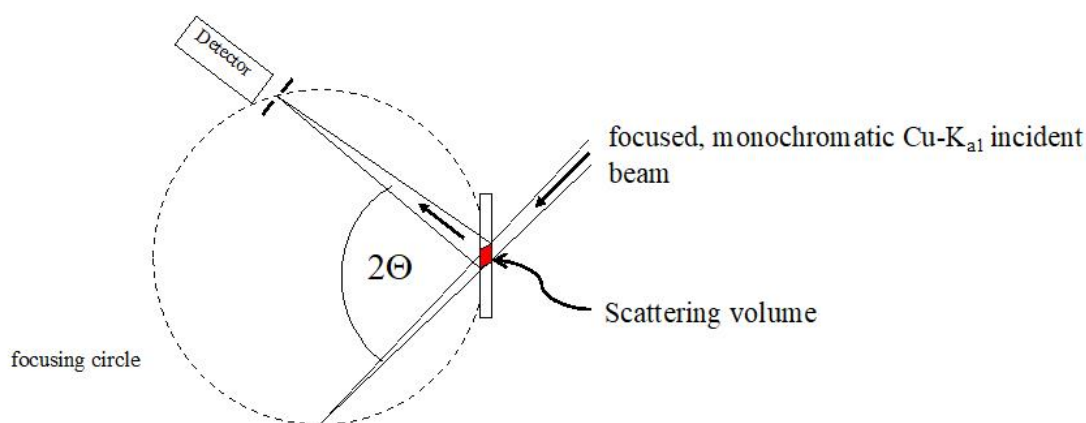


**Figure S1:** Schematic sketch of the Guinier system in transmission (usually angle of incidence set to 45°).

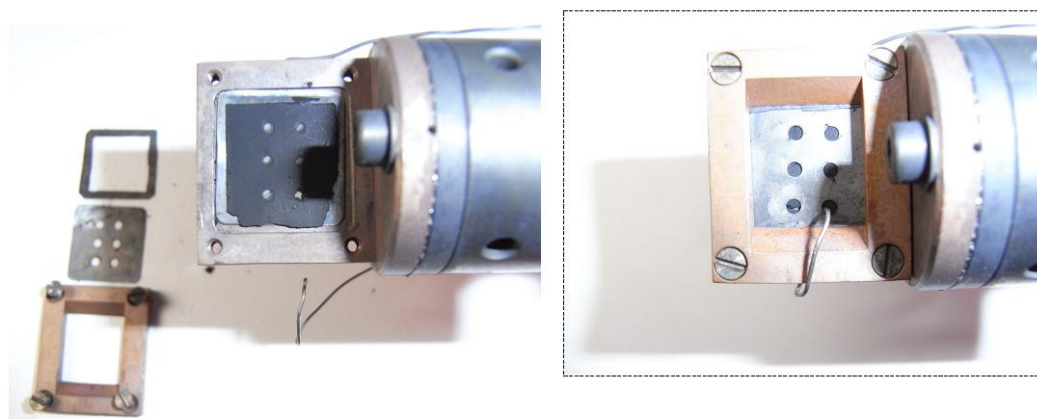
## Details of the self-designed *in situ* cell and sample preparation

Figure S2 is a photo of the reaction cell assembly, with connections for water cooling, two mantel thermocouples, mantel heater connections, and gas-in and gas-out connection plus valves.

The whole device is connected to an outer cylinder at the upper flange, which serves as mechanical support and as an evacuated Dewar bottle.



**Figure S2:** Details of the *in-situ* cell in use for the *Guinier* system. The separately shown cylindrical cup made of Beryllium defines the volume ( $\approx 115$  ml) of the reaction cell. It will be attached to the lower water-cooled flange. Note the circular groove, etched down to a thickness of 0.3 mm to allow for the transmission of the X-ray beam.



**Figure S3:** Details of sample holder: **Left side:** sample inserted (black sheet  $\approx 15.5 \times 11.5$  mm, slightly compressed into a  $\approx 0.2$  mm pellet,  $\approx 55$  mg). The pellet will be sandwiched between two 0.1 mm thick, perforated (1.5 mm) Beryllium platelets. The platelets keep the sample fixed to its position and also serve as thermal conductors between frame and sample. One of the two mantel thermocouples (0.5 mm diameter) is inserted into a hole in the sample holder frame.

**Right side:** fully assembled sample holder. The tip of the second thermocouple is in direct contact with the sample pellet through a hole in the Beryllium platelet. The high purity beryllium platelets produce three very narrow peaks in the diffractograms, which can be easily cut out, but may even be used for accurate angular calibration.

### The Guinier system overview

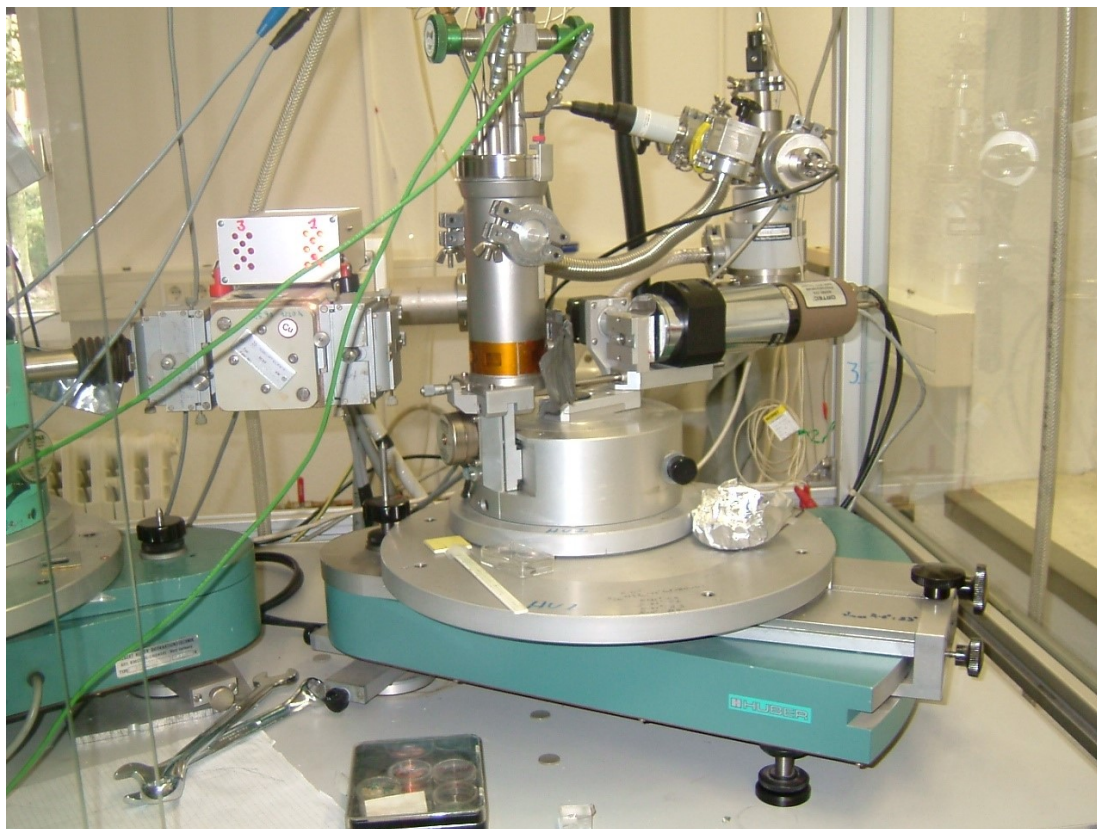


**Figure S4:** Total view of the Guinier systems. The base system is made by the German company HUBER. It was modified to replace of the standard sample holder by a self-designed *in situ* cell (right side). A second Guinier system (left front) is used for experiments under ambient conditions and standard sample holders. All necessary mechanical movements are performed by computer-controlled stepper motors: scanning motor, receiving slit motor, sample exchange motor. A remote operated temperature controller (WEST) allows to run a temperature ramp manually or computer controlled at a preselected ramp rate.

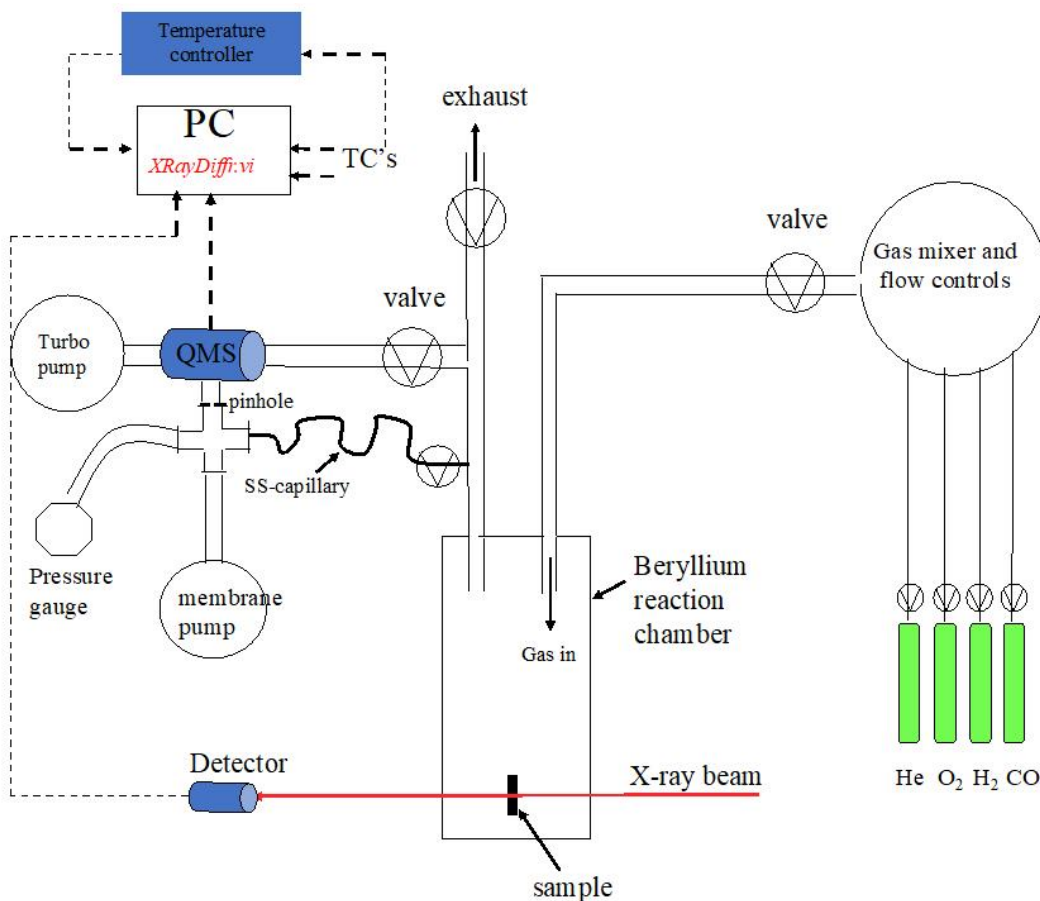


**Figure S5:** Schematic sketch of gas flow system including the quadrupole mass spectrometer (VG, ARGAs) attached to the reaction cell via a differentially pumped stainless steel capillary, lowering the pressure from 1 bar down to  $\approx 100$  mb.

A  $10 \mu\text{m}$  pinhole connects to the QMS. The reaction cell can be evacuated to a base pressure of  $10^{-3}$  mb through the QMS.

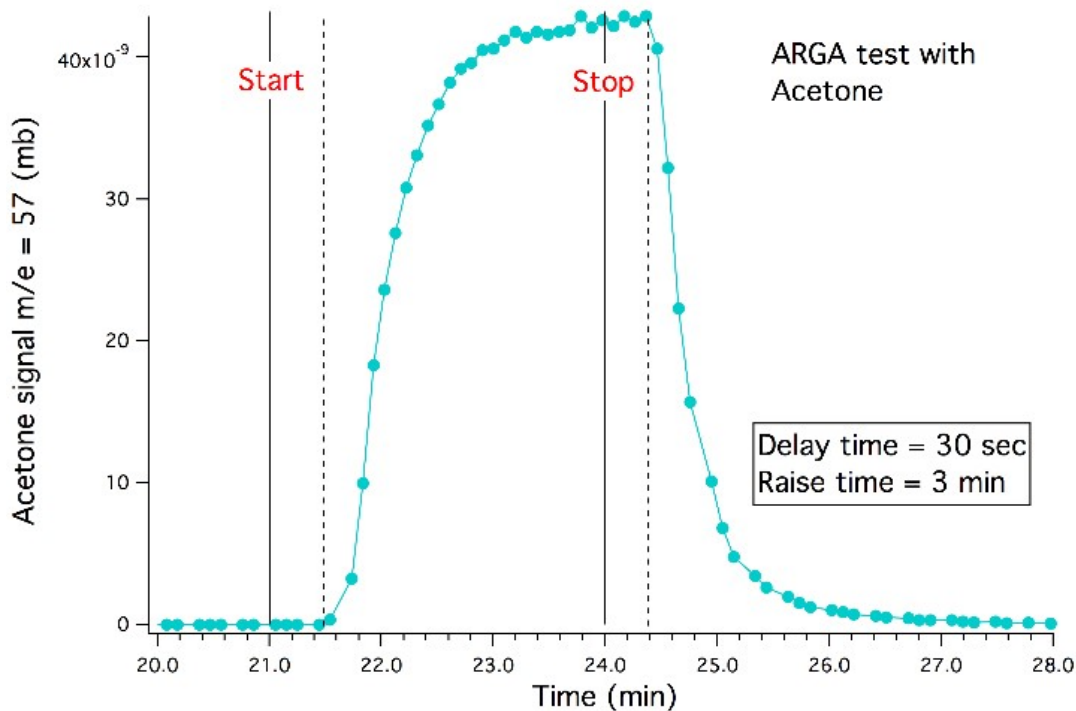


**Figure S6:** Test of the ARGAs response time: the time it takes from a gas supply (here acetone) at the entrance of the capillary to a full response to the QMS. A small delay of 30 s for the QMS response, and a total of  $\approx 3$  min raise time was found. The signal drops from maximum to 10% within  $\approx 40$  s.

## The operating software

The whole system is controlled by a self-designed software *XRayDiffract* using LabView programming. It allows three modes of operation:

**Scan mode:** The sample should be in a stationary state. Step-scanning at preselected time, scanning at start, stop, and step width. The sample holder can adopt two different pellets, e.g. a catalyst and its corresponding pure support material. Sample exchange at every theta-step is made by a recursive shift of the whole reaction chamber in direction parallel to the sample surface. This design allows for an accurate background correction and extraction of the XRD signal of the active catalyst component. XRD raw data are finally corrected for the known angular factors: absorption, dispersion, geometry.

**Open Slit Treatment mode:** The detector is placed at a fixed angle, usually at a strong Bragg peak, and the receiving slit opened to an appropriate width, e.g.  $\Delta\theta = 1^\circ$ . Here we call it the “Bragg-Window”. Changes in the intensity in this window are connected to the treatment conditions. Count rates in the order of  $10^4$  (c/s) are high enough to measure changes at a preselected time interval of 10s. The software collects the I-signal (count rate), two T-signals (temperature of the thermocouple), and up to 5 different QMS-signals for every time step.

Thermal expansion does affect the Bragg peak position and might distort the recorded data. This will be discussed separately<sup>13</sup>

**Fast Scan Treatment Mode:** Similar to the previous mode, but repeated fast scans over a small preselected angular scattering range.

## Estimate of the Pt particle mean spacing inside the ETEK catalyst

From the pellets physical data given along with Figure S3 we get a pellet density of  $\approx 0.5 \text{ g/cm}^3$ , with 20 wt.% Pt we have  $0.01 \text{ g/cm}^3$  Pt, or (with a Pt density of  $21 \text{ g/cm}^3$ ) a total Pt volume  $V = 0.01/21 = 4.7 \times 10^{-4} \text{ cm}^3$ . If we consider a particle size of 3 nm, or a volume of  $v \approx 30 \times 10^{-21} \text{ cm}^3$ , the number  $N$  of particles in one  $\text{cm}^3$  is  $N = V/v \approx 10^{16}$ . To arrive at a mean distance of Pt particles we assume a catalyst cube of edge length 1 cm, and for simplicity the particles to be arranged within it in cubic primitive lattice. Then we have  $N^{1/3} \approx 10^5$  particles along one edge of the cube. The spacing between 3 nm particles would then be roughly  $\approx 10^{-5} \times 10^7 = 100 \text{ nm}$ .

<sup>1</sup>For 3 nm Pt particles and 8 keV photons absorption loss is  $< 0.0013$ .

<sup>2</sup>Integrated in reciprocal space, scale,  $b = 2\sin\Theta/\lambda$ ,  $\Theta$ : Bragg angle,  $\lambda$ : Wavelength.

<sup>3</sup>Throughout this paper, the I-signal is shown as black noisy curve.

<sup>4</sup>The receiving slit was set to  $\Theta = 19.85 \pm 0.5^\circ$ .

<sup>5</sup>The thermal QMS-drift was compensated through dividing  $p(\text{H}_2)$  by the total pressure.

<sup>6</sup>The temperature measured at the sample holder frame.

<sup>7</sup>Under an inert ambient one would expect an increase of the I-signal during heating.

<sup>8</sup>Diffusion limitation will delay the  $p(\text{CO}_2)$ -signal.

<sup>9</sup>We have kept the total flow of the reactants fixed in this experiment, in order to avoid any effect to the  $\text{CO}_2$  partial pressure.

<sup>10</sup>The delay is always equal, about 5 min, and certainly caused by diffusion limitations.

<sup>11</sup>10 sec is the time resolution in this experiment.

<sup>12</sup>Effectively  $\approx 13$  s, delayed by stepper motors and data read out.

<sup>13</sup>Platinum linear thermal expansion coefficient is  $c = 8.8 \cdot 10^{-6} \text{ (K}^{-1}\text{)}$ , and the lattice constant is  $a = a_0(1 + c(\Delta T))$ .

The peak position in reciprocal b-scale is  $b = 1/a = b_0(1 - c(\Delta T))$ , with  $b = 2\sin\Theta/\lambda$ ,  $\Theta$  = Bragg angle,  $\lambda = 1.5406 \text{ \AA}$   
 Say a heat treatment to  $\Delta T = 300 \text{ K}$  is performed. Then the (negative) peak shift remains very small,  $\Delta b/b_0 = -2.5 \cdot 10^{-3}$ .  
 This could only lower the I-signal insignificantly during heating.

## References

1. J Singh, EMC Alayon, M Tromp, OV Safonova, P Glatzel, M Nachtegaal, R Frahm and JA V Bokhoven (2008) *Angew Chem Int. Ed.*, 47: 9260
2. H Over, YD Kim, AP Seitsonen, S Wendt, E Lundgren et al., (2000) *Science* 287: 1474
3. J Gustafson et al., (2008) *ASC Catal.* 8: 5, 4438
4. K Qadir et al., (2012) *Nano Lett* 12: 11, 5761
5. MD Ackermann, TM Pedersen, BLM Hendriksen, O Robach, SC Bobaru et al., (2005) *Phys Rev Lett* 95: 255505
6. FJ Gracia, L Bollmann, EE Wolf, JT Miller and AJ Kropf (2003) *J Catal* 220: 382
7. TH Lindstrom and TT Tsotsis (1986). *Surface Sci*, 171: 349
8. TH Lindstrom and TT Tsotsis (1985) *Surf. Sci.*, 150: 487
9. D Albisson et al., (2021) *ASC Catal* (2021) 11: 4
10. JA Anderson, *J Chem Soc* (1992). *Fraraday Trans*, 88: 1197
11. PA Carlsson, VP Zhdanov and M Skoglundh (2006). *Phys. Chem. Chem. Phys.*, 8: 2703
12. N Hartmann, R Imbihl and W Vogel, *Catal Lett* (1994) 28: 373
13. S Nikitenko, AM Beale, AMJ vd Eerden, SDM Jacques, O Leynaud et al., (2008) *J Synchrotron Rad* 15: 632
14. Mv Laue, *Z Krist* (1926) 64: 115
15. AJC Wilson (1943). *Proc Roy Soc (London) (A)*, 181: 360
16. CR Perrey, CB Carter, J Bentley and M Lentzen, *Microsc Microanal* (2003) 9: 412
17. W Vogel, S Botti, S Martelli and E Carlino, *New J Chem* (1998) 22: 749
18. W Vogel, V Le Rhun, E Garnier and N Alonso-Vante, *J. Phys. Chem. B* (2001) 105: 5238
19. W Vogel and N Alonso-Vante, *J Catal* (2005) 232: 395
20. W Vogel (2008) *J Phys Chem C*, 112: 13475
21. I Langmuir (1992) *Trans Faraday Soc*, 17: 607
22. T Engel and G Ertl (1979) *Adv Catal*, 28: 1
23. MP Cox, G Ertl and R Imbihl (1985) *Phys Rev Lett* 54: 1725
24. M Eiswirth, R J Schwankner and G. Ertl (1985) *Z Phys Chem* 144: 59
25. RJ Schwankner, MEiswirth, P Möller, K Wetz and G Ertl (1987) *J Chem. Phys.*, 87: 742

26. G Ertl (1990) *Adv. Catal.*, 37: 21
27. G Ertl, PR Norton and J Rüstig (1982) *Phys. Rev. Lett.*, 49: 177
28. MA van Spronsen, JWM. Frenken and IMN Groot (2017) *Nature Communication* 8: 429
29. F Garcaia-Martinez et al., (2020) *Angew Chemie Int. Ed.* 59: 45
30. S Oh, S Back, WH Doh, SY Moon, J Kim (2017) *RSC Adv.* 7: 45003
31. E Lashina et al. (2023) *Catalysts* 13: 568
32. JE Turner and MB Maple (1984) *Surf. Sci.*, 147: 647
33. JE Turner, BC Sales and MB Maple (1981) *Surf. Sci.*, 103: 54.
34. W Vogel (1998) *Cryst. Res. Technol.*, 33: 1141
35. F Dassenoy, W Vogel and N Alonso-Vante (2002) *J. Phys. Chem. B*, 106: 12152
36. Z Hou, B Yi and H Zhang (2003) *Electrochem. Solid-State Lett.*, 6: A232
37. B-J Hwang, LS Sarma, JM Chen, CH Chen, SC Shih GR Wang et.al., (2005) *J. Am. Chem. Soc.*, 127: 11140
38. J Prabhuram, TS Zhao, CW Wong and JW Guo (2004) *J. Power Sources*, 134: 1
39. H.-W Wang, R-X Dong, H-Y Chang, C-L Liu and Y-W Chen-Yang (2007). *Materials Lett.*, 61: 830
40. RJ Berry (1978) *Surf Sci*, 76: 415
41. BC Sales, JE Turner and M B Maple (1981) *Surf. Sci.*, 112: 272
42. M R Tinsley, A F Taylor, Z Huang and K Showalter (2009) *Phys. Rev. Lett.* 102: 158301
43. R Kopelman (1988) *Science*, 241: 1620
44. DJ Kaul and EE Wolf (1985). *J Catal*, 93: 321
45. J-B Donnet, R C Bansal and M-J Wang (1993). *Carbon black: science and technology*, Chapter 3, 1993
46. E Clement, P Leroux-Hugon, LM Sander and P Argyrakis (1994) *J. Phys. Chem.*, 98: 1214
47. IZ Kiss, Y Zhai and JL Hudson (2022) *Science* 296: 1676
48. SD Monte, F d'Ovidio, H Chate and E Mosekilde (2004) *Phys. Rev. Lett.*, 92: 254101